

# Quasi-normal modes of quantum gravity black hole with perfectly fluid dark matter

Arpita Jana,\* Manjari Dutta,† and Sunandan Gangopadhyay‡

Department of Astrophysics and High Energy Physics,  
S. N. Bose National Centre for Basic Sciences, JD Block,  
Sector-III, Salt Lake City, Kolkata-700 106, India

In this work, we have studied the motion of a massless scalar photon in the renormalization group (RG) improved Schwarzschild black hole spacetime in the presence of perfectly fluid dark matter (PFDM). Considering the critical orbit conditions and the null geodesics condition in static spherically sym- In metric geometry, we have shown the variation of the radius of the photon sphere  $r_{ph}$  with the PFDM parameter  $\zeta$ . Due to perturbations in black hole spacetime, gravitational waves are emitted in the form of quasi-normal radiations, which correspond to quasi-normal modes (QNMs). In this work, we have studied two types of perturbations in RG improved Schwarzschild spacetime: scalar field perturbations and electromagnetic (EM) field perturbations. For both cases, we have studied the effect of the PFDM parameter on the quasi-normal mode frequencies and the shadow of the black hole, which is related to the photon radius.

## I. INTRODUCTION

Black holes are the most fascinating and mysterious predictions of Einstein's theory of general relativity[1, 2]. The first experimental confirmation of the prediction of GR was the observation of light deflection during the solar eclipse in 1919. Actually, the gravitational force of a black hole is so intense that any object moving around it within a certain radius falls into it. These effects have a combined name called *gravitational lensing* [3–11]. After a century of first observations of light deflection due to gravity, the existence of the black holes has also been verified in some recent observations [12–15] by the LIGO and VIRGO observatories in collaboration with the Event Horizon Telescope (EHT). They published the image of the shadow of a supermassive M87 black hole [13–15]. If light passes close to a black hole, the rays can either be deflected or can travel on a circular orbit. Thus, the light coming from a source behind the black hole can cast a shadow of the black hole on a certain plane, which is visible to a distant observer. Theoretical analyses of black hole shadow have been started in [16] for spherically symmetric black holes. Later in [17], the formation of shadows for spherically symmetric black holes surrounded by accretion disks has been studied. The analysis for the shadow of rotating black holes has been discussed in [18, 19]. In [19–23], the first idea of observing a black hole shadow was produced by numerical simulations. Since then, with the improvements in observational data, various studies on black hole shadows have been done in modified theories of gravity and wormholes as well as higher dimensional gravity theories [24–59]. The study of black hole spacetime and the motion of any particle moving in its vicinity has impactful insights on the features of black holes, such as the Hawking tem-

perature. Particles moving in the black hole spacetime follow the geodesics, in the absence of external forces. The geodesics around any black hole can form closed or open orbits which may be stable or unstable depending on the potential barrier experienced by the particles. The stability of the orbits can be understood by using the Lyapunov exponents [60, 61]. These exponents can be expressed in terms of the second order derivative of the effective potential barrier at extrema [62]. The evolution of a binary black hole system proceeds through three distinct phases: inspiral, merger, and ring-down. The inspiral phase provides information about the mass and spin, using post-Newtonian approximation [63]. The merger phase describes the collapse of two objects leading to the formation of black holes [64–66]. The final phase describes the perturbed black hole emitting gravitational waves (GW) in terms of quasi-normal radiation [67]. This perturbations influence the black hole spacetime and its stability. The frequencies of these perturbations are named as *quasi-normal frequencies (QNF)* and corresponding modes are known as *quasi-normal modes (QNM)*. Several analytical and numerical studies of QNMs have been done in [68–91]. In this paper, we have considered two types of field perturbations in the RG improved Schwarzschild black hole spacetime. First one is the scalar field perturbations and the second one is the electromagnetic field perturbations. We have studied the effects of these fields on black hole spacetime individually in the presence of PFDM. Due to these perturbations, the forms of effective potential barrier change accordingly for both scalar and EM fields. Using these forms, we have studied the effect of PFDM on the QNFs which are related to the effective potential calculated at  $r_{ph}$ . Considering the null geodesics and circular orbit condition, we have shown the variation of the size of the photon sphere  $r_{ph}$  with PFDM parameter  $\zeta$ . Along with these, we have presented a comparison study between the quasi-normal frequencies of two types of field perturbations in the above mentioned black hole geometry in the presence of PFDM.

The arrangement of the paper is as follows. In section

\*Electronic address: [janaarpita2001@gmail.com](mailto:janaarpita2001@gmail.com)

†Electronic address: [chandromouli15@gmail.com](mailto:chandromouli15@gmail.com)

‡Electronic address: [sunandan.gangopadhyay@gmail.com](mailto:sunandan.gangopadhyay@gmail.com)

II, we have presented a basic review of the geodesics of a massless scalar photon in a static, spherically symmetric black hole spacetime, leading to the equation for the photon radius. In section III, we have discussed the theoretical construction of black hole shadow and its relation with the photon sphere. In section IV, we have presented the derivation of the metric of Schwarzschild black hole in the presence of PFDM and then we have provided the brief description of renormalization group improvement of the metric. In section V, we have revisited the derivation of quasi-normal frequencies for spherically symmetric black hole geometries and presented the effect of PFDM parameter on the effective potential for both scalar and electromagnetic perturbations. In section VI, we have presented the effect of PFDM on QNFs and black hole shadow, by plotting the parameters against the PFDM parameter ( $\zeta$ ). In the final section, we have discussed the important findings of this work.

## II. TRAJECTORY OF A PHOTON IN SPHERICALLY SYMMETRIC STATIC SPACETIME

The metric of a static spherically symmetric black hole in (3+1)-dimension can be written as

$$ds^2 = -f(r)dt^2 + f(r)^{-1}dr^2 + r^2(d\theta^2 + \sin^2\theta d\phi^2) \quad (1)$$

where  $f(r)$  denotes the lapse function of the black hole. To study about the geodesics of a massless photon in this geometry, we shall start with the Lagrangian of the system which has the form

$$\mathcal{L} = \frac{1}{2}g_{\mu\nu}\dot{x}^\mu\dot{x}^\nu \quad (2)$$

where the partial derivatives are defined with respect to the affine parameter  $\lambda$ . Trajectories of any massless particle in any spacetime geometry correspond to the null geodesics which satisfy the geodesic condition

$$g_{\mu\nu}\dot{x}^\mu\dot{x}^\nu = 0. \quad (3)$$

In order to obtain the general trajectory of photon in the black hole spacetime, we need to use the separability approach of the Hamilton-Jacobi equation mentioned in [55, 92]. The Hamilton-Jacobi equation with spacetime metric  $g_{\mu\nu}$  has the general form as [92]

$$\frac{\partial S}{\partial \lambda} = -\frac{1}{2}g^{\mu\nu}\frac{\partial S}{\partial x^\mu}\frac{\partial S}{\partial x^\nu} \quad (4)$$

where  $\lambda$  is the affine parameter. The Hamilton-Jacobi action  $S$  can be written as

$$S = \frac{1}{2}m^2\lambda - Et + L\phi + S_r(r) + S_\theta(\theta) \quad (5)$$

to separate the equations of motion for different coordinates.

For photon ( $m = 0$ ), using eq.(4) and eq.(30), we obtain

$$\frac{r^2E^2}{f(r)} - r^2f(r)\left(\frac{\partial S_r}{\partial r}\right)^2 = \left(\frac{\partial S_\theta}{\partial \theta}\right)^2 + \frac{L^2}{\sin^2\theta}. \quad (6)$$

Here, we have used the metric components from eq.(1);  $g^{tt} = -\frac{1}{f(r)}$ ,  $g^{rr} = f(r)$ ,  $g^{\theta\theta} = \frac{1}{r^2}$  and  $g^{\phi\phi} = \frac{1}{r^2\sin^2\theta}$ . Introducing the separation constant  $\mathcal{K}$ , we obtain from eq.(6)

$$\begin{aligned} \left(\frac{\partial S_r}{\partial r}\right)^2 &= \frac{E^2}{(f(r))^2} - \frac{\mathcal{K}^2}{r^2f(r)}, \\ \left(\frac{\partial S_\theta}{\partial \theta}\right)^2 &= \mathcal{K} - \frac{L^2}{\sin^2\theta}. \end{aligned} \quad (7)$$

We have considered the static and spherically symmetric geometry. Since the metric is independent of  $t$  and  $\phi$  coordinates, the generalized momenta corresponding to these are conserved. Now to obtain the trajectory of the photon in the black hole spacetime, we shall use the generalized momentum,  $p_\mu = \frac{\partial S}{\partial x^\mu} = g_{\mu\nu}\frac{dx^\nu}{d\lambda}$ . Hence the equations of motion of the photon obtained as

$$\begin{aligned} \frac{dt}{d\lambda} &= \frac{E}{f(r)}, & \frac{dr}{d\lambda} &= \frac{1}{r^2}\sqrt{(E^2r^4 - \mathcal{K}r^2f(r))}, \\ \frac{d\theta}{d\lambda} &= \frac{1}{r^2}\sqrt{\left(\mathcal{K} - \frac{L^2}{\sin^2\theta}\right)}, & \frac{d\phi}{d\lambda} &= \frac{L}{r^2\sin^2\theta}. \end{aligned} \quad (8)$$

The radial geodesics can be expressed as

$$\left(\frac{dr}{d\lambda}\right)^2 - V(r) = 0 \quad (9)$$

where  $V(r) = E^2\left(1 - \frac{\mathcal{K}f(r)}{r^2E^2}\right)$  and it is called the effective radial potential. We need to find the critical orbit for the photon from the unstable condition

$$V(r = r_{ph}) = 0, \quad \frac{\partial V}{\partial r}\bigg|_{r=r_{ph}} = 0, \quad \frac{\partial^2 V}{\partial r^2}\bigg|_{r=r_{ph}} < 0 \quad (10)$$

where  $r_{ph}$  is the radius of the critical orbit which is called the photon sphere. We shall study the null geodesics here. Hence using the conditions mention in eq.(10), we can obtain

$$\frac{2}{r_{ph}}f(r_{ph}) - f'(r_{ph}) = 0. \quad (11)$$

Here  $f'(r_{ph})$  denotes the derivative of  $f(r)$  with respect to  $r$  at  $r = r_{ph}$ . Solving eq.(11) for any black hole geometry, we can get the expression for the radius of the photon sphere.

Now using eq.(3) and eq.(11), we can obtain the ratio of angular momentum and the energy of the photon as

$$\frac{L}{E} = \frac{r_{ph}}{\sqrt{f(r_{ph})}}. \quad (12)$$

### III. BLACK HOLE SHADOW: CONSTRUCTION AND RELATION WITH PHOTON SPHERE

In this section, we shall discuss the construction of black hole shadow and how it is related with the photon sphere. The detailed explanation about the construction of black hole shadow is described in [11].

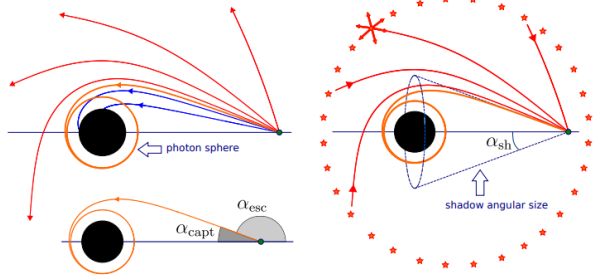


FIG. 1: Construction of black hole shadow [11].

The light rays approaching a black hole from a distant source can follow two distinct trajectories : some are scattered and escape to infinity after being deflected by the gravitational field of the black hole; while others are trapped and fall through the event horizon of the black hole. The critical boundary separating these two behaviors defines the photon sphere where light orbits the black hole under the intense gravitational force. Now, consider an idealized scenario in which light sources are uniformly distributed throughout the universe, except in the region between the observer and the black hole. In this case, only the deflected light rays can reach the observer, while those captured by the event horizon cannot. Consequently, the region corresponding to the captured rays appears dark to the observer. This dark area constitutes the shadow of the black hole.

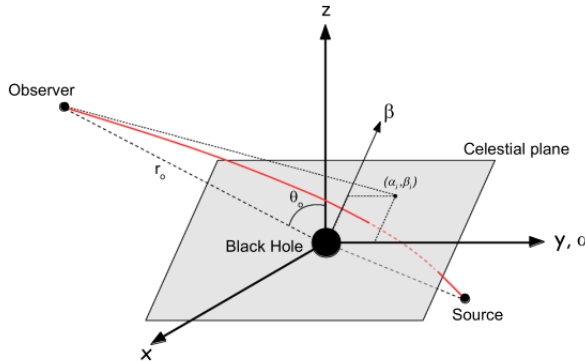


FIG. 2: Diagram for celestial coordinates  $\alpha$  and  $\beta$  [48].

To obtain the size of the black hole shadow, we have to write down the celestial coordinates  $\alpha$  and  $\beta$  [93]. In (3+1)-dimension, for a distant observer, the celestial co-

ordinates are defined as [94]

$$\alpha = \lim_{r \rightarrow \infty} -r^2 \sin \theta \frac{d\phi}{dr} \Big|_{r_{ph}, \theta=\pi/2},$$

$$\beta = \lim_{r \rightarrow \infty} r^2 \frac{d\theta}{dr} \Big|_{r_{ph}, \theta=\pi/2}. \quad (13)$$

Here  $r$  is the distance between the black hole and the observer,  $\alpha$  is the apparent perpendicular distance of the shadow from the symmetry axis and  $\beta$  denotes the apparent perpendicular distance of the shadow from its projection on the equatorial plane. For the reference, see the Fig.(2) taken from [48].

Using the equations of motion mentioned in eq.(8), we obtain

$$\frac{d\phi}{dr} = \frac{L}{\sin^2 \theta \sqrt{E^2 r^4 - \mathcal{K} r^2 f(r)}},$$

$$\frac{d\theta}{dr} = \sqrt{\frac{\mathcal{K} - \frac{L^2}{\sin^2 \theta}}{E^2 r^4 - \mathcal{K} r^2 f(r)}}. \quad (14)$$

Now using eq.(14) and eq.(13) and taking the limit  $r \rightarrow \infty$ , we obtain the celestial coordinates as

$$\alpha = -\frac{L}{E}, \quad \beta = \sqrt{\frac{\mathcal{K}}{E^2}}. \quad (15)$$

The radius of the black hole shadow in  $\alpha$ - $\beta$  plane is

$$R_s = \sqrt{\alpha^2 + \beta^2} = \sqrt{\xi^2 + \eta} \quad (16)$$

where  $\xi = \frac{L}{E}$  and  $\eta = \frac{\mathcal{K}}{E^2}$ . Using the critical orbit condition eq.(10), it is obtained that

$$\xi^2 + \eta = \frac{r_{ph}^2}{f(r_{ph})}. \quad (17)$$

Now combining eq.(16) and eq.(17), we obtain the shadow radius as

$$R_s = \frac{r_{ph}}{\sqrt{f(r_{ph})}}. \quad (18)$$

This equation defines the direct relationship between the photon radius  $r_{ph}$  and the shadow radius of a black hole  $R_s$ .

### IV. STABILITY ANALYSIS OF PHOTON ORBIT : LYAPUNOV EXPONENT

In this section, we shall discuss the brief review of the Lyapunov exponent.

Lyapunov exponents measure the average rate of convergence or divergence of nearby trajectories in phase-space. A positive Lyapunov exponent denotes a chaotic system and a negative Lyapunov exponent denotes a stable system. To study the geodesic analysis in terms of Lyapunov

exponents, we shall start with equation of motion of a dynamical system given by [95]

$$\frac{dY_i}{dt} = G_i(Y_j) . \quad (19)$$

Perturbing the system slightly, we can have (upto linear order)

$$\frac{d(\delta Y_i(t))}{dt} = K_{ij}(t)\delta Y_j(t) \quad (20)$$

where  $K_{ij}$  is called the *linear stability matrix* [96], defined as

$$K_{ij}(t) = \frac{\partial G_i}{\partial Y_j} \Big|_{Y_i(t)} . \quad (21)$$

The solution of eq.(20) is written as

$$\delta Y_i(t) = L_{ij}(t)\delta Y_j(t=0) \quad (22)$$

with  $L_{ij}$  being the *evolution matrix* [95] which obeys  $L_{ij}(t=0) = \delta_{ij}$ .

The eigenvalues of the linear stability matrix  $K_{ij}$  give the Lyapunov exponents  $\lambda$  which determines the stability of the system.

We are interested in the circular orbit of a massless photon in an equatorial plane. The analysis will be carried out in the phase-space  $(p_r, r)$  for coordinate time  $t$ . The Euler-Lagrange equation for  $r$  is given by

$$\frac{d}{d\lambda} \left( \frac{\partial \mathcal{L}}{\partial \dot{r}} \right) - \frac{\partial \mathcal{L}}{\partial r} = 0 . \quad (23)$$

Here  $\dot{r} = \frac{dr}{d\lambda}$  and the generalized momentum is given by

$$p_r = \frac{\partial \mathcal{L}}{\partial \dot{r}} . \quad (24)$$

Using the above equations, we obtain

$$\begin{aligned} \frac{dr}{dt} &= \frac{\dot{r}}{\dot{t}} \\ \frac{dp_r}{dt} &= \frac{\dot{p}_r}{\dot{t}} . \end{aligned} \quad (25)$$

Now the system is perturbed with  $r \rightarrow r + \delta r$  and  $p_r \rightarrow p_r + \delta p_r$  and we obtain

$$\delta p_r = \left( \frac{\partial^2 \mathcal{L}}{\partial \dot{r}^2} \right) \delta \dot{r} \quad (26)$$

and since  $\dot{t}$  is fixed on circular orbit, we get

$$\begin{aligned} \delta \left( \frac{dr}{dt} \right) &= \frac{1}{\dot{t}} \left( \frac{\partial^2 \mathcal{L}}{\partial \dot{r}^2} \right)^{-1} \delta p_r \\ \delta \left( \frac{dp_r}{dt} \right) &= \frac{1}{\dot{t}} \frac{d}{dr} \left( \frac{\partial \mathcal{L}}{\partial r} \right) \delta r . \end{aligned} \quad (27)$$

We can write the above set of equations in matrix form as

$$\frac{d}{dt} \begin{pmatrix} \delta p_r \\ \delta r \end{pmatrix} = \begin{bmatrix} 0 & \frac{1}{\dot{t}} \frac{d}{dr} \left( \frac{\partial \mathcal{L}}{\partial r} \right) \\ \frac{1}{\dot{t}} \left( \frac{\partial^2 \mathcal{L}}{\partial \dot{r}^2} \right)^{-1} & 0 \end{bmatrix} \begin{pmatrix} \delta p_r \\ \delta r \end{pmatrix} . \quad (28)$$

This matrix is the linear stability matrix and to find the Lyapunov exponents we, need to find the eigenvalues of the matrix evaluated on the photon sphere  $r_{ph}$ . Hence the Lyapunov exponent becomes

$$\lambda^2 = \frac{1}{g_{rr}\dot{t}^2} \frac{d}{dr} \left( \frac{\partial \mathcal{L}}{\partial r} \right) \Big|_{r=r_{ph}} = \frac{\left( \frac{d^2 V}{dr^2} \right)}{2\dot{t}^2} \Big|_{r=r_{ph}} . \quad (29)$$

Here, we have used  $\dot{r}^2 = V(r)$  and the critical orbit condition mentioned in eq.(10).

## V. RENORMALIZATION GROUP IMPROVEMENT OF SCHWARZSCHILD BLACK HOLE IMMERSED IN PFDM

This section is based on the derivation of the metric for Schwarzschild black hole in the presence of PFDM and the RG improvement of this metric.

### A. Schwarzschild black hole in the presence of PFDM

Here we consider the (3+1)-dimensional gravity theory in the presence of PFDM [97, 98]. The action can be written as

$$I = \int d^4x \sqrt{-g} \left( \frac{R}{16\pi G} + \mathcal{L}_{PFDM} \right) \quad (30)$$

where  $\mathcal{L}$  is the Lagrangian density due to the presence of PFDM,  $G$  is the Newton's gravitational constant and  $R$  is the Ricci scalar. Extremizing the action, we can get the corresponding equations of motion as

$$R_{\mu\nu} - \frac{1}{2}g_{\mu\nu}R = -8\pi G T_{\mu\nu}^{PFDM} \quad (31)$$

with  $R_{\mu\nu}$  being the Ricci scalar and  $T_{\mu\nu}^{PFDM}$  being the energy-momentum tensor for the PFDM medium. The energy-momentum tensor for PFDM has the form [94, 99, 100]

$$(T^\mu{}_\nu)^{PFDM} = diag(-\rho, P_r, P, P) ; P_r = -\rho \quad (32)$$

with  $\rho$  and  $P$  being the energy density and the pressure of the medium respectively. In order to find the equation of state of the PFDM, we shall use the approach mentioned in [99, 101] and hence we consider [94]

$$\begin{aligned} (T^\theta{}_\theta)^{PFDM} &= (T^t{}_t)^{PFDM}(1-\epsilon) \\ (T^\phi{}_\phi)^{PFDM} &= (T^r{}_r)^{PFDM}(1-\epsilon) \end{aligned} \quad (33)$$

<sup>1</sup> All overdots denote the derivative with respect to the affine parameter  $\lambda$ .

where  $\epsilon$  is a constant. Substituting eq.(32) into eq.(33), the equation of state for PFDM is obtained as [99]

$$\frac{P}{\rho} = (\epsilon - 1) . \quad (34)$$

There can be many choices for the value of  $\epsilon$  [101] but in our case, we have chosen  $\epsilon = \frac{3}{2}$  [101, 102]. Hence the equation of state of perfectly fluid dark matter becomes

$$\frac{P}{\rho} = \frac{1}{2} . \quad (35)$$

To solve the Einstein field equations, we shall take an ansatz for a static, spherically symmetric metric [94]

$$ds^2 = -e^{\sigma(r)}dt^2 + e^{\gamma(r)}dr^2 + r^2(d\theta^2 + \sin^2\theta d\phi^2) . \quad (36)$$

Using eq.(31) and eq.(36), we obtain the equations as [94]

$$\begin{aligned} e^{-\gamma}\left(\frac{1}{r^2} - \frac{\gamma'}{r}\right) - \frac{1}{r^2} &= -8\pi G\rho, \\ e^{-\gamma}\left(\frac{1}{r^2} + \frac{\sigma'}{r}\right) - \frac{1}{r^2} &= -8\pi G\rho, \\ \frac{e^{-\gamma}}{2}\left(\sigma'' + \frac{\sigma'^2}{2} + \frac{\sigma' - \gamma'}{r} - \frac{\sigma'\gamma'}{2}\right) &= 8\pi GP, \\ \frac{e^{-\gamma}}{2}\left(\sigma'' + \frac{\sigma'^2}{2} + \frac{\sigma' - \gamma'}{r} - \frac{\sigma'\gamma'}{2}\right) &= 8\pi GP . \end{aligned} \quad (37)$$

In the above equations, prime and double prime denotes first and second derive with respect to  $r$ . Now, taking the ratio of the first and the third equations and using eq.(35), we obtain

$$\frac{e^{-\gamma}}{2}\left(\sigma'' + \frac{\sigma'^2}{2} + \frac{\sigma' - \gamma'}{r} - \frac{\sigma'\gamma'}{2}\right) = -\frac{1}{2}\left\{e^{-\gamma}\left(\frac{1}{r^2} - \frac{\gamma'}{r}\right) - \frac{1}{r^2}\right\} . \quad (38)$$

Now subtracting the first two equations in eq.(37), we obtain

$$\sigma' + \gamma' = 0 \Rightarrow \sigma + \gamma = 0 \quad (39)$$

where the integration constant has been set to zero.

We now define  $\sigma(r) = \ln(1 - B(r))$  and hence substituting it in eq.(38), we get

$$r^2 B'' + 3r B' + B = 0 . \quad (40)$$

Solving this equation, we obtain

$$B(r) = \frac{r_s}{r} - \frac{\zeta}{r} \ln\left(\frac{r}{|\zeta|}\right) \quad (41)$$

with  $r_s$  and  $\zeta$  being the integration constant. Setting  $\zeta = 0$  and using weak field approximation, we obtain  $r_s = 2GM$ .

Comparing eq.(1) and eq.(36), the lapse function of the black hole is obtained as

$$f(r) = e^{\sigma(r)} = (1 - B(r)) = 1 - \frac{2GM}{r} + \frac{\zeta}{r} \ln\left(\frac{r}{|\zeta|}\right) . \quad (42)$$

Here  $M$  is the mass of the black hole and  $\zeta$  represents the intensity of the PFDM medium [94].

## B. Metric for RG improved Schwarzschild black hole in the presence of PFDM

As it is expected that the theory of general relativity would break down at very small length scale due to its nonrenormalizability [103, 104], the developing theory of quantum gravity is one of the fascinating topics to the researchers. One of the schemes is the asymptotic safety scenario which is based on the renormalization group (RG) approach [105–107]. In 2000, Bonanno and Reuter [108], first applied this approach in a Schwarzschild black hole background, where they replaced the usual Newton's gravitational constant with the running gravitational constant. These type of renormalization group improved black holes are named as *quantum corrected black holes*. The methods to achieve such quantum improved geometry have been discussed elaborately in [108–111]. The first step is to obtain the momentum scale-dependent coupling constants from the renormalization group flow equations; while the next step is to write down the momentum cut-off scale in terms of the radial coordinates of spherically symmetric geometry. There are mostly used two ways to do the scale identification, one of which is based on constructing curvature scalars like Ricci scalar and Kretschmann scalar, while the other method is based on the UV fixed point which separates the weak-coupling and strong-coupling regime. The third step to achieve the geometry has to done in three possible ways. Firstly, one can directly impose the flowing coupling constants into the classical solution to improve that. Secondly, one can put the running coupling constants in the equation of motion; such as we can get the quantum improved Einstein field equation by imposing running gravitational constant and running cosmological constant

$$G_{\mu\nu} = 8\pi G(x)T_{\mu\nu} - \Lambda(x)g_{\mu\nu} \quad (43)$$

where the flow of the matter coupling has been ignored. The final approach is to impose the running couplings in the action level. The quantum improved Lagrangian density for Einstein-Hilbert action can be written as

$$\mathcal{L} = \frac{\sqrt{-g}}{16\pi G(x)}(R - 2\Lambda(x)) . \quad (44)$$

The simplest way to achieve the geometry is to impose running couplings into the solution level<sup>2</sup>. This was a quick revisit of quantum corrected geometries.

For a quantum corrected Schwarzschild black hole, the lapse function can be written as

$$f(r) = 1 - \frac{2G(r)M}{r} \quad (45)$$

where  $G(r)$  is running gravitational constant. The flow of Newton's gravitational constant  $G$  has been originated

<sup>2</sup> In this paper, all the analyses have been executed for  $\Lambda = 0$ .

from the renormalization group flow equation [108, 112, 113]

$$k \frac{d\tilde{G}(k)}{dk} = 2\tilde{G}(k) \left( 1 - \frac{\tilde{G}(k)}{4\pi\tilde{\alpha}} \right) \quad (46)$$

with  $\tilde{G}(k)$  being the dimensionless Newton's constant, defined as  $\tilde{G}(k) = k^2 G(k)$  and  $\tilde{\alpha}$  is a constant which corresponds to the fixed point  $\tilde{G}_* = 4\pi\tilde{\alpha}$ . Integrating eq.(46) within the limit 0 and  $k$ , we obtain the flow of Newton's gravitational constant in terms of momentum cut-off scale as [114]

$$G(k) = \frac{4\pi\tilde{\alpha}G}{4\pi\tilde{\alpha} + k^2G} \quad (47)$$

Using the method of cut-off identification in terms of radial coordinate [112, 113], the position dependent flow of Newton's gravitational constant reads

$$G(r) = \frac{G}{1 + \frac{\tilde{\omega}G}{r^2}} \quad (48)$$

$\tilde{\omega}$  is the quantum gravity parameter.

Now the lapse function eq.(45) takes the form

$$f(r) = 1 - \frac{2GMr}{(r^2 + \tilde{\omega}G)} \quad (49)$$

Hence, the metric for quantum corrected Schwarzschild black hole in the presence of PFDM can be written down using eq.(42) and eq.(49) as

$$f(r) = 1 - \frac{2GMr}{(r^2 + \tilde{\omega}G)} + \frac{\zeta}{r} \ln \left( \frac{r}{|\zeta|} \right) \quad (50)$$

This is the metric which we shall use in our further analysis of this work.

## VI. QUASI-NORMAL MODES OF A FIELD FOR QUANTUM CORRECTED SCHWARZSCHILD BLACK HOLE SURROUNDED BY PFDM

In this section, we shall discuss about the perturbation of the static, spherically symmetric black hole geometry

in the presence of a scalar field and electromagnetic field individually.

### A. Scalar perturbations

The massless scalar field  $\Phi$  in curved spacetime follows the Klein-Gordon equation

$$\frac{1}{\sqrt{-g}} \partial_\mu (\sqrt{-g} g^{\mu\nu} \partial_\nu \Phi) = 0 \quad (51)$$

Here  $\sqrt{-g} = r^2 \sin \theta$  which is found from the determinant of the (3+1)-dimensional spacetime metric mentioned in eq.(1). The ansatz for the solution is given in terms of the spherical harmonics and has the form [115-117]

$$\Phi(t, r, \theta, \phi) = e^{-i\omega t} Y_{l,m}(\theta, \phi) \frac{\psi(r)}{r} \quad (52)$$

with  $l = 0, 1, 2, \dots$  being called as multipole number. After imposing separation of variables, the scalar field perturbation equation can be recast as

$$\frac{f(r)}{r^2} \frac{d}{dr} \left[ r^2 f(r) \frac{d}{dr} \left( \frac{\psi(r)}{r} \right) \right] + \left( \omega^2 - f(r) \frac{l(l+1)}{r^2} \right) \frac{\psi(r)}{r} = 0 \quad (53)$$

Now defining tortoise coordinate  $r_*$  by the definition  $\frac{dr_*}{dr} = \frac{1}{f(r)}$ , eq.(53) takes the form of Schrödinger-like wave equation with potential  $V(r_*)$

$$\frac{d^2\psi}{dr_*^2} + (\omega^2 - V(r_*)) \psi = 0 \quad (54)$$

where  $V(r_*)$  has the following form

$$V(r_*) = f(r) \left( \frac{l(l+1)}{r^2} + \frac{f'(r)}{r} \right) \quad (55)$$

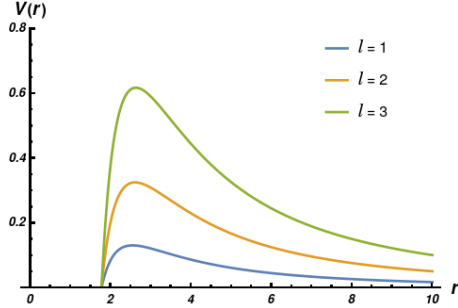
Substituting the form of the lapse function  $f(r)$  from eq.(50), we get the effective potential as

$$\begin{aligned} V(r) &= \left( 1 - \frac{2GMr}{(r^2 + \tilde{\omega}G)} + \frac{\zeta}{r} \ln \left( \frac{r}{|\zeta|} \right) \right) \times \left( \frac{l(l+1)}{r^2} + \frac{2GM(r^2 - \tilde{\omega}G)}{r(r^2 + \tilde{\omega}G)^2} + \frac{\zeta}{r^3} \left( 1 - \ln \left( \frac{r}{|\zeta|} \right) \right) \right) \\ &\approx \frac{l(l+1)}{r^2} + \frac{1}{r^3} \left[ (l(l+1) - 1) \left( \zeta \ln \left( \frac{r}{|\zeta|} \right) - 2GM - 1 \right) \right] + \frac{1}{r^4} \left[ 4GM\zeta \left( \ln \left( \frac{r}{|\zeta|} \right) - \frac{1}{2} \right) - \zeta^2 \ln \left( \frac{r}{|\zeta|} \right) \left( \ln \left( \frac{r}{|\zeta|} \right) - 1 \right) \right] \\ &\quad + \frac{2}{r^5} G^2 M \tilde{\omega} (l(l+1) - 3) + \frac{1}{r^6} \left[ 16G^3 M^2 \tilde{\omega} - 8G^2 M \tilde{\omega} \zeta \left( \ln \left( \frac{r}{|\zeta|} \right) - \frac{1}{4} \right) \right] \end{aligned} \quad (56)$$

In Fig.(3), we have plotted the effective potential  $V(r)$

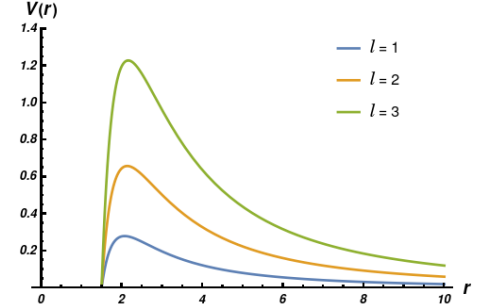
versus  $r$  for scalar field perturbations. To plot this, we

have set  $\tilde{\omega} = 0.01$ . It is clear from the plot that increasing the value of  $l$  increases the height of the potential. Two



(a) Effective potential for  $l = 1, 2, 3$  ( $\zeta = 0.07$ )

plots are for two different values of PFDM parameter  $\zeta$  and for large value of  $\zeta$ , potential has higher peak.



(b) Effective potential for  $l = 1, 2, 3$  ( $\zeta = 0.80$ )

FIG. 3: Comparison of effective potentials for scalar field perturbations for  $l = 1, 2, 3$  at different values of  $\zeta$ .

Since, eq.(54) is similar to the one-dimensional Schrödinger equation, we shall use the WKB approximation method to solve this and this can be expressed in the form of

$$\frac{d^2\psi(x)}{dx^2} + Q(x)\psi(x) = 0. \quad (57)$$

In the black hole perturbation equation,  $\psi$  represents the radial part of the wavefunction. In eq.(57),  $x$  denotes the tortoise coordinate  $r_*$  which ranges from  $-\infty$  to  $+\infty$  and  $Q(x) \equiv (\omega^2 - V(r_*))$ , which is constant at  $x \rightarrow \pm\infty$ .

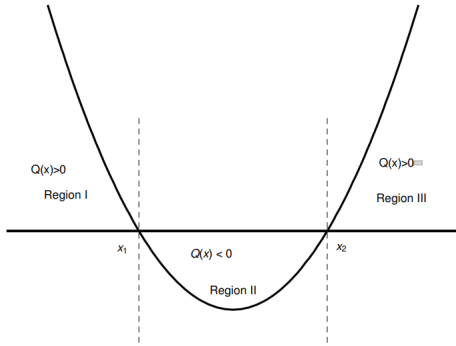


FIG. 4: behaviour of  $Q(x)$  [100, 118].

$Q(x)$  follows the behaviour shown in Fig.(4). The semi-analytical WKB approximation has been used in [69] to solve this problem.

The WKB approximation method is used to solve a system with slowly varying potential; which means the potential remains almost constant over a region of the order of the de-Broglie wavelength. To solve eq.(57), we consider a trial form for  $\psi(x)$  in terms of amplitude  $A(x)$

and a phase factor  $\theta(x)$ <sup>3</sup>[118, 119]

$$\psi(x) = A(x)e^{i\theta(x)}. \quad (58)$$

The amplitude  $A(x)$  changes slowly with  $x$ . Using eq. (57) and (58), we obtain the solution for  $\psi(x)$  in the region where  $Q(x) > 0$  as [69, 118, 119]

$$\psi(x) = \frac{1}{(Q(x))^{\frac{1}{4}}} \exp\left(\pm i \int_x^{x_1} \sqrt{Q(x')} dx'\right); \quad (\text{Region I}) \quad (59)$$

$$\psi(x) = \frac{1}{(Q(x))^{\frac{1}{4}}} \exp\left(\pm i \int_{x_2}^x \sqrt{Q(x')} dx'\right); \quad (\text{Region III}) \quad (60)$$

Assuming that the two turning points  $x_1$  and  $x_2$  are closely aligned that means  $x_1 \simeq x_2 = x_0$ ,  $Q(x)$  can be approximated as a parabola in region II where  $Q(x) < 0$ . Hence,  $Q(x) = Q_0 + \frac{1}{2}(x - x_0)^2 \frac{d^2Q}{dx^2}|_{x=x_0} + \dots$  where  $Q_0 \equiv Q(x_0) < 0$ ,  $Q'(x_0) = 0$  and  $Q''(x_0) > 0$ . Now eq.(57) can be written in the following form

$$\frac{d^2\psi}{dx^2} + \left(Q_0 + \frac{1}{2}Q''_0(x - x_0)^2\right)\psi(x) = 0. \quad (61)$$

Solving the above equation, we shall be able to obtain the form of  $\psi(x)$  in the region where  $Q(x) < 0$ . To find the exact solution, we shall use the parabolic cylinder functions [120]. Now defining

$$\begin{aligned} \kappa &\equiv \frac{1}{2}Q''_0, \quad q \equiv (4\kappa)^{1/4}e^{i\pi/4}(x - x_0), \\ \mu + \frac{1}{2} &\equiv \frac{-iQ_0}{\sqrt{2Q''_0}} \end{aligned} \quad (62)$$

<sup>3</sup> This  $\theta$  and the spherical coordinate  $\theta$  mentioned in eq. (1) are not same.

we can rewrite eq. (61) in the following form

$$\frac{d^2\psi}{dq^2} + \left(\mu + \frac{1}{2} - \frac{q^2}{4}\right)\psi(q) = 0. \quad (63)$$

Solutions of this equation are parabolic cylinder functions  $D_\mu(q)$ . Now, following the method used in [120] we obtain the solution as

$$\psi(q) \equiv D_\mu(q) = C_1 q^\mu e^{-q^2/4} + C_2 q^{-\mu-1} e^{q^2/4}. \quad (64)$$

Since only asymptotic solutions are expected, hence,  $e^{q^2/4}$  term will blow up with  $C_2$  being zero and  $C_1 = 1$ . Now to know the complete asymptotic expansion of  $D_\mu(q)$ , we consider

$$D_\mu(q) = q^\mu e^{-q^2/4} w(q) \quad (65)$$

with  $w(q)$  having an asymptotic power series in the order of  $\frac{1}{q}$ . Substituting eq.(65) into eq.(63) and using the method of power series, the asymptotic expansion ( $q \rightarrow \infty$ ) of  $w(q)$  reads [120]

$$w(q) = 1 - \frac{\mu(\mu-1)}{2q^2} + \frac{\mu(\mu-1)(\mu-2)(\mu-3)}{8q^4} + \dots \quad (66)$$

Now  $D_\mu(q)$  can be written in terms of the linear combinations of the other two solutions of eq.(63)

$$D_\mu(q) = aD_\mu(-q) + bD_{-\mu-1}(-iq). \quad (67)$$

Replacing  $q$  with  $iq$ , above equation takes the form

$$D_\mu(iq) = aD_\mu(-iq) + bD_{-\mu-1}(q). \quad (68)$$

Now using eq.(65),(66) and (68), the forms of the two constant coefficients  $a$  and  $b$  can be found as<sup>4</sup>

$$a = e^{i\mu\pi}, \quad b = \frac{\sqrt{2\pi}}{\Gamma(-\mu)} e^{i(\mu+1)\pi/2}. \quad (69)$$

In asymptotic limit, the required form of wavefunction would be  $\psi \sim e^{-i\mathcal{B}(x-x_0)^2}$  where  $\mathcal{B}$  is some function of  $Q(x)$  which is a constant in asymptotic limit. Hence in eq.(68), the second term has to be zero and hence  $\Gamma(-\mu) = \infty$  that means  $\mu$  to be any positive integer  $n$ . Now using eq.(62) and  $Q(x) \equiv (\omega^2 - V(r))$  we get the expression for quasi-normal frequency  $\omega$  as

$$\omega^2 = V(r_0) - i(n + \frac{1}{2})\sqrt{-2V''(r_0)}, \quad n = 0, 1, 2, \dots \quad (70)$$

where  $r_0$  represents the extrema of the potential  $V(r)$ .

### B. Electromagnetic perturbations

In this subsection, we shall discuss the electromagnetic perturbation in spherically symmetric black hole spacetime (eq.(1)). The EM field in curved spacetime is governed by the Maxwell's equations

$$\nabla_\mu F^{\mu\nu} = 0 \quad (71)$$

where  $F^{\mu\nu}$  is the EM field tensor which is defined by

$$F_{\mu\nu} = \partial_\mu A_\nu - \partial_\nu A_\mu \quad (72)$$

with  $A_\mu$  being the electromagnetic potential. Hence the wave equation for EM field reads [115]

$$\frac{1}{\sqrt{-g}} \partial_\nu (\sqrt{-g} g^{\alpha\mu} g^{\sigma\nu} (\partial_\alpha A_\sigma - \partial_\sigma A_\alpha)) = 0. \quad (73)$$

$A_\mu$  in spherically symmetric black hole background can be expanded in four-dimensional vector spherical harmonics as [80, 121, 122]

$$A_\mu(t, r, \theta, \phi) = \sum_{l,m} \left( \begin{bmatrix} 0 \\ 0 \\ \frac{a_{l,m}(t,r)}{\sin \theta} \partial_\phi Y_{l,m}(\theta, \phi) \\ -a_{l,m}(t,r) \sin \theta \partial_\theta Y_{l,m}(\theta, \phi) \end{bmatrix} + \begin{bmatrix} g_{l,m}(t,r) Y_{l,m}(\theta, \phi) \\ h_{l,m}(t,r) Y_{l,m}(\theta, \phi) \\ k_{l,m}(t,r) \partial_\theta Y_{l,m}(\theta, \phi) \\ k_{l,m}(t,r) \partial_\phi Y_{l,m}(\theta, \phi) \end{bmatrix} \right). \quad (74)$$

Here, the axial part (first term) has  $(-1)^{l+1}$  parity and the polar part (second term) has  $(-1)^l$  parity.

Considering axial and polar perturbations individually, we obtain the wave equation from eq.(73) and (74) as

$$\frac{d^2\psi}{dr_*^2} + (\omega^2 - V(r_*)) \psi = 0 \quad (75)$$

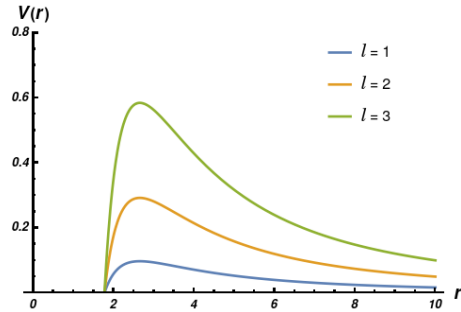
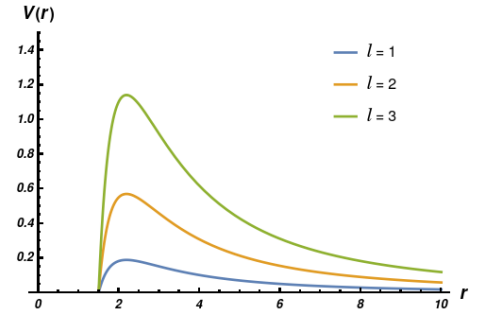
where  $r_*$  is the tortoise coordinate as defined earlier and  $V(r)$  is the effective potential for EM perturbations which has the form

$$V(r) = f(r) \frac{l(l+1)}{r^2}. \quad (76)$$

In our case, the effective potential takes the form as

$$V(r) = \left(1 - \frac{2GMr}{(r^2 + \tilde{\omega}G)} + \frac{\zeta}{r} \ln\left(\frac{r}{|\zeta|}\right)\right) \times \frac{l(l+1)}{r^2}. \quad (77)$$

Fig.(5) shows the nature of the effective potential  $V(r)$  for electromagnetic perturbations. It is obvious that these are also of same nature as for the scalar perturbation was (Fig.(3)). The heights of the potential barriers are slightly less in compared to the scalar field perturbations.

(a) Effective potential for  $l = 1, 2, 3$  ( $\zeta = 0.07$ )(b) Effective potential for  $l = 1, 2, 3$  ( $\zeta = 0.80$ )FIG. 5: Comparison of effective potentials for electromagnetic field perturbations for  $l = 1, 2, 3$  at different values of  $\zeta$ .

The wave functions for axial and polar perturbations have the forms [80, 115]

$$\begin{aligned}\psi_a(t, r) &= a_{l,m}(t, r) , \\ \psi_p(t, r) &= \frac{r^2}{l(l+1)} (\partial_t h_{l,m}(t, r) - \partial_r g_{l,m}(t, r)) .\end{aligned}\quad (78)$$

Now, following the WKB method mentioned in the earlier subsection, we can write the quasi-normal frequency for EM perturbations in terms of the effective potential same as eq.(70).

## VII. THE EFFECT OF PFDM ON SHADOW RADIUS AND QNF

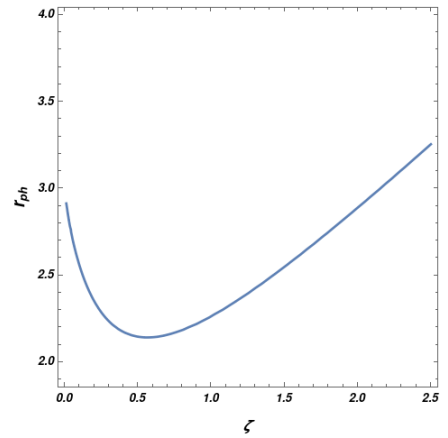
In this section, we shall discuss the relation between the quasi-normal frequencies and the shadow radius and how they are affected by the PFDM.

Using the critical orbit conditions (eq.(10)), the equation for photon radius  $r_{ph}$  for spherically symmetric black hole is obtained in eq.(11). Considering the lapse function of RG improved Schwarzschild black hole mentioned in eq.(50), we can recast eq.(11) as

$$2r_{ph}^3 + \left[ \zeta \left\{ 3 \ln \left( \frac{r_{ph}}{|\zeta|} \right) - 1 \right\} - 6GM \right] r_{ph}^2 + 10G^2 M \tilde{\omega} = 0 \quad (79)$$

where we have taken only the linear order of  $\tilde{\omega}$ .

Being a transcendental equation, it is difficult to solve the above equation analytically to find the exact expression of  $r_{ph}$ . In Fig.(6), we have plotted the photon radius  $r_{ph}$  against the PFDM parameter  $\zeta$ , setting  $\tilde{\omega} = 0.01$ . Initially  $r_{ph}$  decreases with increasing  $\zeta$  and after reaching a minima, it starts increasing.

FIG. 6: Variation of  $r_{ph}$  with  $\zeta$ .

The shadow of the black hole is formed due to the deflection of light in its vicinity. The expression for the shadow radius follows from eq.(18).

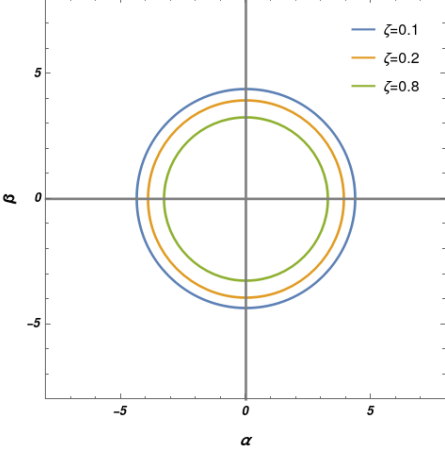
$\zeta$	$R_S$
0.1	4.34832
0.2	3.91577
0.5	3.35368
0.6	3.28651
0.8	3.24119
1.0	3.27035
1.2	3.34430
1.4	3.44694
1.6	3.56889
1.8	3.70442
2.0	3.84980

TABLE I: Variation of  $R_S$  with respect to  $\zeta$ .

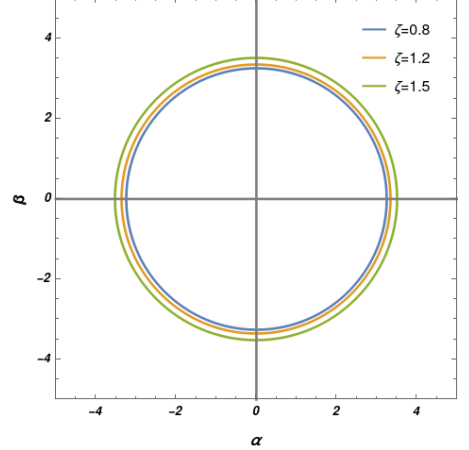
For quantum corrected Schwarzschild black hole surrounded by PFDM, the expression for the shadow radius

is

$$R_s = \frac{r_{ph}}{\sqrt{1 - \frac{2GMr_{ph}}{(r_{ph}^2 + \bar{\omega}G)} + \frac{\zeta}{r_{ph}} \ln\left(\frac{r_{ph}}{|\zeta|}\right)}} \simeq \frac{\sqrt{3}r_{ph} \left[1 - \frac{12G^2M\bar{\omega}}{r_{ph}^3(1 + \frac{\zeta}{r_{ph}})}\right]}{\sqrt{1 + \frac{\zeta}{r_{ph}}}}. \quad (80)$$



(a) Black hole shadow for different  $\zeta \leq 0.8$



(b) Black hole shadow for different  $\zeta \geq 0.8$

FIG. 7: Effect of PFDM parameter on the black hole shadow

Now we shall discuss the relation between this photon radius and quasi-normal frequency.

Since, on the photon sphere ( $r = r_{ph}$ ), effective potential has the maxima, we can write eq.(70) as

$$\omega^2 = V(r_{ph}) - i(n + \frac{1}{2})\sqrt{-2V''(r_{ph})} \equiv A - iB \quad (81)$$

where  $A = V(r_{ph})$  and  $B = (n + \frac{1}{2})\sqrt{-2V''(r_{ph})}$ . Now we can consider the expression for QNF as

$$\omega = \omega_R - i\omega_I \quad (82)$$

with  $\omega_R$  and  $\omega_I$  being the real part and the imaginary part of the QNF respectively.

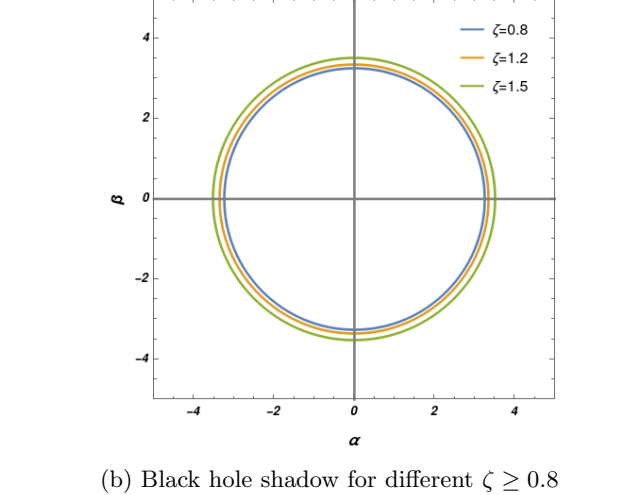
Taking the square of eq.(82) and comparing with eq.(81), expressions for  $\omega_R$  and  $\omega_I$  can be obtained as

$$\omega_R = \sqrt{\frac{A + \sqrt{A^2 + B^2}}{2}}, \quad \omega_I = \frac{B}{\sqrt{2(A + \sqrt{A^2 + B^2})}}. \quad (83)$$

Using the expression of  $A$  and  $B$  mentioned in eq.(81), we obtain the forms of real and imaginary parts of quasi-

In the final expression, the logarithmic term  $\ln\left(\frac{r_{ph}}{|\zeta|}\right)$  has been replaced using eq.(79), keeping contributions only up to first order in  $\bar{\omega}$ .

In Fig.(7), we have shown the effect of PFDM parameter  $\zeta$  on the radius of black hole shadow. It is clear from the plot and Table I that at  $\zeta = 0.8$ , the size of the shadow is minimum, after which the shadow radius starts increasing with  $\zeta$ .



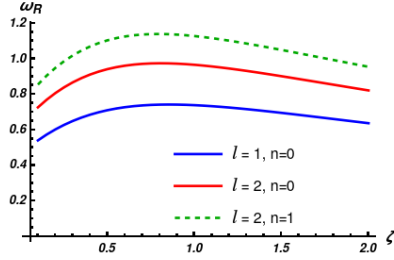
normal frequency in terms of the effective potential as

$$\omega_R = \sqrt{\frac{V(r_{ph}) + \sqrt{V^2(r_{ph}) - 2(n + \frac{1}{2})V''(r_{ph})}}{2}}, \quad \omega_I = \frac{(n + \frac{1}{2})\sqrt{-2V''(r_{ph})}}{2\left(V(r_{ph}) + \sqrt{V^2(r_{ph}) - 2(n + \frac{1}{2})V''(r_{ph})}\right)}. \quad (84)$$

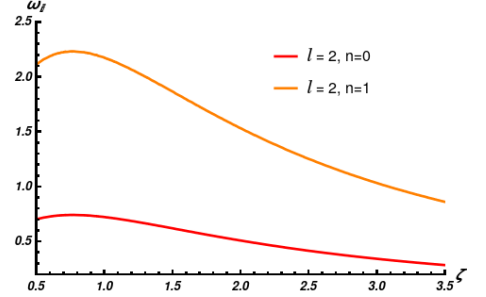
In Fig.(8), we have plotted  $\omega_R$  and  $\omega_I$  against the PFDM parameter  $\zeta$  for different values of  $l$  and  $n$ . It is shown that both  $\omega_R$  and  $\omega_I$  has maxima and then decreases with increasing  $\zeta$ . We plotted  $\omega_R$  for different values of  $l$  and  $n$ . For large  $l$ , the peak is higher and between the plots for  $l = 2$ , large  $n$  gives the higher peak. In the plot of  $\omega_I$  (Fig.(8b)), higher  $n$  value shows the higher peak of quasi-normal frequency.

$\zeta$	$\omega(l = 2, n = 0)$	$\omega(l = 2, n = 1)$
0.5	$0.9422 - 0.7053i$	$1.1043 - 2.1159i$
0.6	$0.9614 - 0.7309i$	$1.1258 - 2.1927i$
0.8	$0.9750 - 0.7438i$	$1.1397 - 2.2315i$
1.0	$0.9665 - 0.7250i$	$1.1281 - 2.1751i$
1.2	$0.9454 - 0.6888i$	$1.1021 - 2.0666i$
1.4	$0.9175 - 0.6444i$	$1.0684 - 1.9333i$
1.5	$0.9022 - 0.6226i$	$1.0501 - 1.8680i$
1.6	$0.8864 - 0.5992i$	$1.0313 - 1.7977i$
1.8	$0.8542 - 0.5537i$	$0.9931 - 1.6611i$
2.0	$0.8222 - 0.5114i$	$0.9551 - 1.5342i$

TABLE II: Variation of  $\omega$  with respect to  $\zeta$  for scalar field perturbation.



(a) Variation of  $\omega_R$  for scalar field perturbation with  $\zeta$



(b) Variation of  $\omega_I$  for scalar field perturbation with  $\zeta$

FIG. 8: Effect of PFDM parameter on the QNF of scalar field perturbation

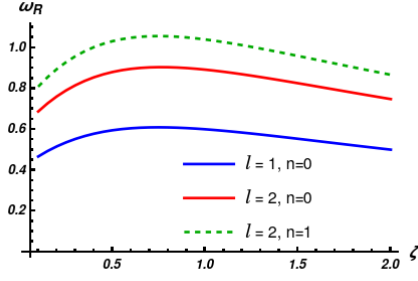
$\zeta$	$\omega(l = 2, n = 0)$	$\omega(l = 2, n = 1)$
0.5	$0.8815 - 0.6158i$	$1.0325 - 1.8476i$
0.6	$0.8969 - 0.6335i$	$1.0494 - 1.9005i$
0.8	$0.9049 - 0.6375i$	$1.0566 - 1.9127$
1.0	$0.8930 - 0.6147i$	$1.0409 - 1.8442i$
1.2	$0.8702 - 0.5783i$	$1.0127 - 1.7349i$
1.4	$0.8418 - 0.5373i$	$0.9784 - 1.6121i$
1.5	$0.8266 - 0.5165i$	$0.9601 - 1.5497i$
1.6	$0.8110 - 0.4960i$	$0.9416 - 1.4881i$
1.8	$0.7797 - 0.4553i$	$0.9043 - 1.3660i$
2.0	$0.7488 - 0.4181i$	$0.8679 - 1.2545i$

TABLE III: Variation of  $\omega$  with respect to  $\zeta$  for electromagnetic field perturbation.

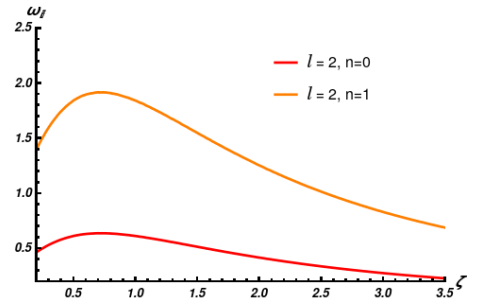
Fig.(9) shows the variations of quasi-normal frequencies

for electromagnetic field perturbations. We have plotted these using eq.(76),(81) and (83). In this case also, both  $\omega_R$  and  $\omega_I$  has certain maxima and then they starts decreasing with increasing PFDM parameter  $\zeta$ . Unlike the previous case, for large  $l$  and  $n$  the peaks of the quasi-normal frequencies are higher.

Table II and Table III present the variation of quasi-normal mode frequency for scalar field and electromagnetic field perturbation respectively. In contrast to the behavior of the shadow radius, the quasi-normal frequencies also exhibit a transition at  $\zeta = 0.8$ . Both the real part  $\omega_R$  and the imaginary part  $\omega_I$  increase initially, attain their maximum values at  $\zeta = 0.8$ , and subsequently decrease beyond this point.



(a) variation of  $\omega_R$  for electromagnetic field perturbation with  $\zeta$

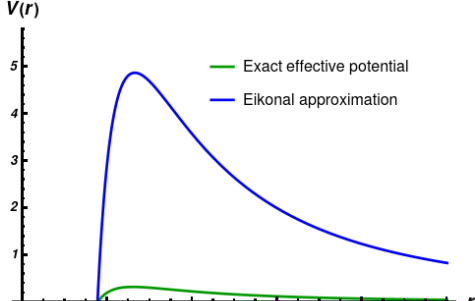


(b) variation of  $\omega_I$  for electromagnetic field perturbation with  $\zeta$

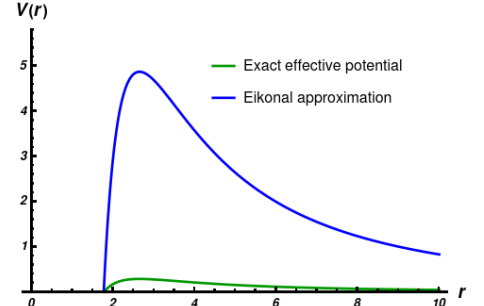
FIG. 9: Effect of PFDM parameter on the QNF of electromagnetic field perturbation

Comparing two plots (Fig.(8) and Fig.(9)), we can see a distinct difference between the two field perturbations. For both the real and imaginary part of the quasi-normal frequency, the peaks are noticeably higher in the case of scalar field perturbation than in the electromagnetic one. To find the direct relation between quasi-normal frequency and the shadow radius, we shall now impose the eikonal approximation ( $l \gg 1$ )<sup>[95]</sup> and the effective potential (eq.(55)) can be approximated as

$$V(r) \approx f(r) \frac{l(l+1)}{r^2}. \quad (85)$$



(a) Scalar field perturbation



(b) Electromagnetic field perturbation

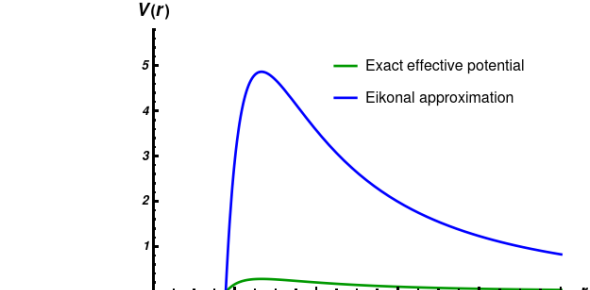
FIG. 10: Comparing the effective potential in exact form and in eikonal approximation. The exact effective potential has been plotted for  $l = 2$  and for eikonal approximation, the plot is for  $l = 10$ .

In Fig.(10), we compare the effective potential  $V(r)$  obtained from its exact expression with that derived under the eikonal approximation. In the eikonal limit, a larger value of  $l$  is considered, resulting in a higher potential peak compared to the exact effective potential, which is plotted for  $l = 2$ . Since in eikonal approximation, the effective potential for both the perturbation has the same form in eq.(85), it results eq.(81) as

$$\omega^2 = l(l+1)\Omega_{ph}^2 - 2i(n + \frac{1}{2})\lambda\Omega_{ph}\sqrt{l(l+1)} \quad (87)$$

For the lapse function mentioned in eq.(50), the effective potential takes the form in eikonal approximation as

$$V(r) \approx \left(1 - \frac{2GMr}{(r^2 + \tilde{\omega}G)} + \frac{\zeta}{r} \ln\left(\frac{r}{|\zeta|}\right)\right) \times \frac{l(l+1)}{r^2}. \quad (86)$$



where  $\Omega_{ph}$  is the orbital velocity of the massless scalar photon, defined by

$$\Omega_{ph} = \frac{d\phi}{dt} \Big|_{r=r_{ph}} = \sqrt{\frac{f(r_{ph})}{r_{ph}^2}}. \quad (88)$$

$\lambda$  in eq.(87) is the Lyapunov exponent<sup>5</sup> which is related

<sup>5</sup> It is different from the affine parameter  $\lambda$  mentioned earlier.

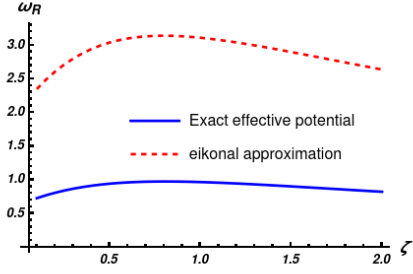
to the second order derivative of effective potential on the photon sphere [95]

$$\lambda = \sqrt{\frac{V''(r)}{2t^2}} \Big|_{r=r_{ph}} . \quad (89)$$

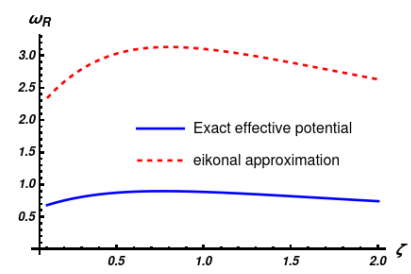
Now in large  $l$  limit, using eq.(83) and (87), a simplified

form of  $\omega$  can be written as

$$\omega = l\Omega_{ph} - i(n + \frac{1}{2})|\lambda| . \quad (90)$$



(a) Scalar field perturbation



(b) Electromagnetic field perturbation

FIG. 11: Comparing the real part of QNF for exact  $V(r)$  and  $V(r)$  in eikonal approximation. The exact effective potential has been plotted for  $l = 2$  and for eikonal approximation, the plot is for  $l = 10$ .

Fig.(11) illustrates the quasi-normal frequencies obtained from the exact effective potential  $V(r)$  alongside those derived using the eikonal approximation. In the eikonal regime, the peaks of the QNF are noticeably higher compared to those corresponding to the exact potential.

Now using eq.(18) and eq.(88), the above expression can be written in terms of shadow radius as

$$\omega = \frac{l}{R_s} - i(n + \frac{1}{2})|\lambda| . \quad (91)$$

Hence, in eikonal regime, the real part of QNF is inversely proportional to the shadow radius. The importance of this relation relies on the fact that one can measure both the quantities from the knowledge of the other.

### VIII. CONCLUSION

In this paper, we have studied the effects of field perturbations in the renormalization group improved Schwarzschild black hole background surrounded by perfectly fluid dark matter (PFDM). We have also discussed the effects of PFDM on the shadow of the black hole.

In section II, we have started with the study of the null geodesics of a massless scalar photon in a static, spherically symmetric geometry and using the conditions of critical orbits, we have written down the equation for the radius of the photon sphere in this geometry. In the following section, we have revisited the discussion on the theoretical basis for the construction of black hole shadow and the relation between the shadow radius  $R_s$  and the radius of the photon sphere  $r_{ph}$ . In section IV, the metric for the Schwarzschild black hole in the presence of PFDM

has been derived and the renormalization group improvement of this metric has been discussed. Our present analysis is based on the metric mentioned in eq.(50), which represents the quantum gravity improved Schwarzschild black hole surrounded by PFDM. Here, the Newton's gravitational constant flows with the momentum cut-off scale, which is originated from the renormalization group flow equation.

In section V, we have two subsections. In the first part, we have considered the scalar field perturbations in the RG improved Schwarzschild black hole spacetime in the presence of PFDM. Using the effective potential in eq.(55), we have showed the nature of  $V(r)$  for different multipole number  $l$ , and for larger  $l$ , the peak of the potential barrier is higher. We have compared the nature of effective potential for  $\zeta = 0.07$  and  $\zeta = 0.8$  and it is clearly shown in Fig.(3), that for large  $\zeta$ , the potential has higher peak.

In the second part, we have considered the electromagnetic field perturbations in the same background. In this case, the effective potential has the form given in eq.(76). As we have done for the scalar field perturbation, here also we have showed the nature of  $V(r)$  for  $l = 1, 2, 3$ . From the plot (Fig.(5)), it is clear that for large  $l$ , the peak of the potential barrier is higher. In this case also, larger value of  $\zeta$  gives the higher peaks of the potential barrier.

In the last section, we have studied the effects of perfectly fluid dark matter on the photon radius and the shadow radius in Fig.(6) and Fig.(7) respectively. The photon radius  $r_{ph}$  starts decreasing initially and after reaching a minima, it starts increasing with PFDM parameter  $\zeta$ . The turning point for  $r_{ph}$  is at  $\zeta \approx 0.8$ , from where it

starts to increase.

We have plotted the shadow radius for two cases. First case is for  $\zeta \leq 0.8$ , while the second one is for  $\zeta \geq 0.8$ . From the plot, it is clear that for  $\zeta = 0.8$ , the size of the shadow is minimum. The reason for such an observation is that  $R_s$  is related to  $r_{ph}$  via eq.(18). In this section, we have also showed the effect of  $\zeta$  on the real and imaginary parts of the quasi-normal frequencies. We have showed the variations of  $\omega_R$  and  $\omega_I$  for both the perturbations with respect to  $\zeta$  for different values of  $l$  and  $n$ .  $\omega_R$  has the higher peak for large  $l$  and for  $l = 2, n = 0$  and  $l = 2, n = 1$  plots, large  $n$  shows the higher peak. Similar nature is observed in the case of imaginary part of

the frequency. There is a distinct difference between the plots for scalar and electromagnetic perturbations. For the electromagnetic field, the frequency peaks are visibly lower than the case for the scalar field. In Fig.(10), we compare the exact effective potential with its eikonal approximation. Since the eikonal limit corresponds to large  $l$ , the peak of the effective potential in this regime is higher than that of the exact potential. A similar analysis is performed for the real part of the QNF in Fig.(11), where we again observe that the transition point in the eikonal limit occurs at a higher value compared to the exact case.

---

[1] A. Einstein, “*Die Feldgleichungen der Gravitation*”, Sitz. Preuß. Akad. Wiss. 844 (1915).

[2] A. Einstein, “*Die Grundlage der allgemeinen Relativitätstheorie*”, *Ann. der Phys. (Berlin)* **354**, 769 (1916).

[3] P. Schneider, J. Ehlers and E.E. Falco, “*Gravitational Lenses*”, Springer-Verlag, Berlin (1992) .

[4] B. D. Blandford and R. Narayan, “*Cosmological applications of gravitational lensing*”, *Annual Rev. Astron. Astrophys.* **30**, 311-358 (1992).

[5] A. Petters, H. Levine and J. Wambsganss, “*Singularity Theory and Gravitational Lensing*”, *Progress in Mathematical Physics*, **21**, Birkhäuser, Boston, MA (2001).

[6] V. Perlick, “*Gravitational Lensing from a Spacetime Perspective*”, *Living Rev. Relativ.* **7**, 9 (2004).

[7] P. Schneider, C.S. Kochanek and J. Wambsganss, “*Gravitational Lensing: Strong, Weak and Micro*”, Springer, Berlin (2006).

[8] M. Bartelmann, “*Gravitational lensing*”, *Class. Quantum Grav.* **27**, 233001 (2010).

[9] S. Dodelson, “*Gravitational lensing*”, Cambridge: Cambridge University Press (2017).

[10] A. B. Congdon and C. Keeton, “*Principles of Gravitational Lensing: Light Deflection as a Probe of Astrophysics and Cosmology*”, Springer, Cham, Switzerland (2018).

[11] V. Perlick and O. Yu. Tsupko, “*Calculating black hole shadows: Review of analytical studies*”, *phys. rep.* **947**, 1-39 (2022).

[12] B. P. Abbott, et. al., “*Observation of Gravitational Waves from a Binary Black Hole Merger*”, *Phys. Rev. Lett.* **116**, 061102 (2016).

[13] K. Akiyama, et. al., “*First M87 Event Horizon Telescope Results. I. The Shadow of the Supermassive Black Hole*”, *Astrophys. J. Lett.* **875**, L1 (2019).

[14] K. Akiyama, et. al., “*First M87 Event Horizon Telescope Results. IV. Imaging the Central Supermassive Black Hole*”, *Astrophys. J. Lett.* **875**, L4 (2019).

[15] K. Akiyama, et. al., “*First Sagittarius A\* Event Horizon Telescope Results. I. The Shadow of the Supermassive Black Hole in the Center of the Milky Way*”, *Astrophys. J. Lett.* **930**, L12 (2022).

[16] J. L. Synge, “*The Escape of Photons from Gravitationally Intense Stars*”, *Monthly Notice the Royal Astronomical Society* **131** (3), 463-466 (1966).

[17] J. P. Luminet, “*Image of a spherical black hole with thin accretion disk*”, *Astron. Astrophys.* **75**, 228-235 (1979).

[18] S. Chandrasekhar, “*The mathematical theory of black holes*”, Oxford University Press, New York, 1992.

[19] H. Falcke, F. Melia and E. Agol, “*Viewing the Shadow of the Black Hole at the Galactic Center*”, *Astrophys. J.* **528**, L13 (2000).

[20] F. Melia and H. Falcke, “*The Supermassive Black Hole at the Galactic Center*”, *Ann. Rev. Astron. and Astrophys.* **39**, 309-352 (2001).

[21] J. M. Bardeen, “*Timelike and null geodesics in the Kerr metric*”, *Black holes (Les astres occlus)* 215-239 (1973).

[22] K. Hioki and K. I. Maeda, “*Measurement of the Kerr spin parameter by observation of a compact object's shadow*”, *Phys. Rev. D* **80**, 024042 (2009).

[23] A de Vries, “*The apparent shape of a rotating charged black hole, closed photon orbits and the bifurcation set A4*”, *Class. Quantum Grav.* **17** (1), 123 (2000).

[24] A. Grenzebach, V. Perlick and C. Lämmerzahl, “*Photon regions and shadows of accelerated black holes*”, *Int. J. Mod. Phys. D* **24** (9), 1542024 (2015).

[25] A. Grenzebach, V. Perlick and C. Lämmerzahl, “*Photon regions and shadows of Kerr-Newman-NUT black holes with a cosmological constant*”, *Phys. Rev. D* **89**, 124004 (2014).

[26] A. Övgün, İ. Sakalli and J. Saavedra, “*Shadow cast and deflection angle of Kerr-Newman-Kasuya spacetime*”, *JCAP* **10**, 041 (2018).

[27] A. Övgün, İ. Sakalli and J. Saavedra, “*Shadow cast of noncommutative black holes in Rastall gravity*”, *Mod. Phys. Lett. A* **35** (20), 2050163 (2020).

[28] S. W. Wei, Y. C. Zou, Yu. X. Liu and R. B. Mann, “*Curvature radius and Kerr black hole shadow*”, *JCAP* **08**, 030 (2019).

[29] A. Abdujabbarov, M. Amir, B. Ahmedov and S. G. Ghosh, “*Shadow of rotating regular black holes*”, *Phys. Rev. D* **93**, 104004 (2016).

[30] M. Wang, S. Chen and J. Jing, “*Shadow casted by a Konoplya-Zhidenko rotating non-Kerr black hole*”, *JCAP* **10**, 051 (2017).

[31] A. K. Mishra, S. Chakraborty and S. Sarkar, “*Understanding photon sphere and black hole shadow in dynamically evolving spacetimes*”, *Phys. Rev. D* **99**, 104080 (2019).

[32] R. Kumar, B. P. Singh and S. G. Ghosh, “*Shadow and deflection angle of rotating black hole in asymptotically*

safe gravity”, *Annals Phys.* **120**, 168252 (2020).

[33] R. Kumar, B. P. Singh, Md. S. Ali and S. G. Ghosh, “Rotating black hole shadow in Rastall theory”, [arXiv:1712.09793 \[gr-qc\]](https://arxiv.org/abs/1712.09793).

[34] R. A. Hennigar, M. B. J. Poshteh and R. B. Mann, “Shadows, signals, and stability in Einsteinian cubic gravity”, *Phys. Rev. D* **97**, 064041 (2018).

[35] H. Khodabakhshi, A. Giaimo and R. B. Mann, “Einstein quartic gravity: Shadows, signals, and stability”, *Phys. Rev. D* **102**, 044038 (2020).

[36] M. Amir and S. G. Ghosh, “Shapes of rotating non-singular black hole shadows”, *Phys. Rev. D* **94**, 024054 (2016).

[37] R. Shaikh, “Black hole shadow in a general rotating spacetime obtained through Newman-Janis algorithm”, *Phys. Rev. D* **100**, 024028 (2019).

[38] E. Contreras, Á. Rincón, G. Panotopoulos, P. Bargueño, and B. Koch, “Black hole shadow of a rotating scale-dependent black hole”, *Phys. Rev. D* **101**, 064053 (2020).

[39] H. Lü and H. D. Lyu, “Schwarzschild black holes have the largest size”, *Phys. Rev. D* **101**, 044059 (2020).

[40] X. H. Feng and H. Lü, “On the size of rotating black holes”, *Eur. Phys. J. C* **80**, 551 (2020).

[41] R. Kumar, S. G. Ghosh, and A. Wang, “Gravitational deflection of light and shadow cast by rotating Kalb-Ramond black holes”, *Phys. Rev. D* **101**, 104001 (2020).

[42] R. Kumar, S. G. Ghosh, and A. Wang, “Shadow cast and deflection of light by charged rotating regular black holes”, *Phys. Rev. D* **100**, 124024 (2019).

[43] L. Ma and H. Lü, “Bounds on photon spheres and shadows of charged black holes in Einstein-Gauss-Bonnet-Maxwell gravity”, *Phys. Letters B* **807**, 135535 (2020).

[44] R. A. Konoplya and A. Zhidenko, “Analytical representation for metrics of scalarized Einstein-Maxwell black holes and their shadows”, *Phys. Rev. D* **100**, 044015 (2019).

[45] S. Dastan, R. Saffari and S. Soroushfar, “Shadow of a Kerr-Sen dilaton-axion Black Hole”, [arXiv:1610.09477\[gr-qc\]](https://arxiv.org/abs/1610.09477).

[46] S. Dastan, R. Saffari and S. Soroushfar, “Shadow of a charged rotating black hole in  $f(R)$  gravity”, *Eur. Phys. J. Plus* **137**, 1002 (2022).

[47] A. Das, A. Saha and S. Gangopadhyay, “Shadow of charged black holes in Gauss-Bonnet gravity”, *Eur. Phys. J. C* **80**, 180 (2020).

[48] A. Saha, S. M. Modumudi and S. Gangopadhyay, “Shadow of a noncommutative geometry inspired Ayón Beato García black hole”, *Gen Relativ Gravit* **50**, 103 (2018).

[49] L. Amarilla and E. F. Eiroa, “Shadow of a rotating braneworld black hole”, *Phys. Rev. D* **85**, 064019 (2012).

[50] L. Amarilla and E. F. Eiroa, “Shadow of a Kaluza-Klein rotating dilaton black hole”, *Phys. Rev. D* **87**, 044057 (2013).

[51] L. Amarilla, E. F. Eiroa and G. Giribet, “Null geodesics and shadow of a rotating black hole in extended Chern-Simons modified gravity”, *Phys. Rev. D* **81**, 124045 (2010).

[52] T. Vetsov, G. Gyulchev and S. Yazadjiev, “Shadows of Black Holes in Vector-Tensor Galileons Modified Gravity”, [arXiv:1801.04592 \[gr-qc\]](https://arxiv.org/abs/1801.04592).

[53] H. M. Wang, Y. M. Xu and S. W. Wei, “Shadows of Kerr-like black holes in a modified gravity theory”, *JCAP* **03**, 046 (2019).

[54] T. Zhu, Q. Wu, M. Jamil and K. Jusufi, “Shadows and deflection angle of charged and slowly rotating black holes in Einstein-Æther theory”, *Phys. Rev. D* **100**, 044055 (2019).

[55] U. Papnoi, F. Atamurotov, S. G. Ghosh and B. Ahmedov, “Shadow of five-dimensional rotating Myers-Perry black hole”, *Phys. Rev. D* **90**, 024073 (2014).

[56] A. Abdjabbarov, F. Atamurotov, N. Dadhich, B. Ahmedov and Z. Stuchlík, “Energetics and optical properties of 6-dimensional rotating black hole in pure Gauss-Bonnet gravity”, *Eur. Phys. J. C* **75**, 399 (2015).

[57] B. P. Singh and S. G. Ghosh, “Shadow of Schwarzschild-Tangherlini black holes”, [arXiv:1707.07125 \[gr-qc\]](https://arxiv.org/abs/1707.07125).

[58] V. Perlick, O. Yu. Tsupko and G. S. Bisnovatyi-Kogan, “Black hole shadow in an expanding universe with a cosmological constant”, *Phys. Rev. D* **97**, 104062 (2018).

[59] P. C. Li, M. Guo and B. Chen, “Shadow of a spinning black hole in an expanding universe”, *Phys. Rev. D* **101**, 084041 (2020).

[60] A. M. Lyapunov, “The General Problem of the Stability of Motion”, Taylor and Francis (1992).

[61] A. Pikovsky and A. Politi, “Lyapunov Exponents: A Tool to Explore Complex Dynamics”, Cambridge University Press, U.K. (2016).

[62] P. Pradhan, “Stability analysis and quasinormal modes of Reissner-Nordstrøm space-time via Lyapunov exponent”, *Pramana - J Phys* **87**, 5 (2016).

[63] L. Blanchet, “Analyzing gravitational waves with general relativity”, *C.R. Phys.* **20**, 507 (2019).

[64] F. Pretorius, “Evolution of Binary Black-Hole Space-times”, *Phys. Rev. Lett.* **95**, 121101 (2005).

[65] M. Campanelli, C. O. Lousto, P. Marronetti, and Y. Zwlochower, “Accurate Evolutions of Orbiting Black-Hole Binaries without Excision”, *Phys. Rev. Lett.* **96**, 111101 (2006).

[66] J. G. Baker, J. Centrella, D.-I. Choi, M. Koppitz, and J. van Meter, “Gravitational-Wave Extraction from an In-spiraling Configuration of Merging Black Holes”, *Phys. Rev. Lett.* **96**, 111102 (2006).

[67] E. Berti, V. Cardoso, and C. Will, “Gravitational-wave spectroscopy of massive black holes with the space interferometer LISA”, *Phys. Rev. D* **73**, 064030 (2006).

[68] V. Ferrari and B. Mashhoon, “New approach to the quasinormal modes of a black hole”, *Phys. Rev. D* **30**, 295 (1984).

[69] B. F. Schutz and C. M. Will, “Black hole normal modes - A semianalytic approach”, *Astrophys. J. Lett.* **291**, L33 (1985).

[70] S. Iyer and C. M. Will, “Black-hole normal modes: A WKB approach. I. Foundations and application of a higher-order WKB analysis of potential-barrier scattering”, *Phys. Rev. D* **35**, 3621 (1987).

[71] R. A. Konoplya, “Quasinormal behavior of the  $D$ -dimensional Schwarzschild black hole and the higher order WKB approach”, *Phys. Rev. D* **68**, 024018 (2003).

[72] R. A. Konoplya and A. Zhidenko, “Quasinormal modes of black holes: From astrophysics to string theory”, *Rev. Mod. Phys.* **83**, 793 (2011).

[73] R. A. Konoplya, “How to tell the shape of a wormhole by its quasinormal modes”, *Phys. Lett. B* **784**, 43 (2018)..

[74] S. Chandrasekhar and S. Detweiler, “The quasi-normal modes of the Schwarzschild black hole”, *Proc. R. Soc. A* **344**, 441 (1975).

[75] E. W. Leaver, “*An analytic representation for the quasi-normal modes of Kerr black holes*”, *Proc. R. Soc. A* **402**, 285 (1985).

[76] G. T. Horowitz and V. E. Hubeny, “*Quasinormal modes of AdS black holes and the approach to thermal equilibrium*”, *Phys. Rev. D* **62**, 024027 (2000).

[77] H. T. Cho, A. S. Cornell, J. Doukas, T.-R. Huang, and W. Naylor, “*A New Approach to Black Hole Quasinormal Modes: A Review of the Asymptotic Iteration Method*”, *Adv. Theor. Math. Phys.* **2012**, 281705 (2012).

[78] K. D. Kokkotas and B. G. Schmidt, “*Quasi-Normal Modes of Stars and Black Holes*”, *Living Rev. Relativ.* **2**, 2 (1999).

[79] E. Berti, V. Cardoso, and A. O. Starinets, “*Quasinormal modes of black holes and black branes*”, *Class. Quantum Grav.* **26**, 163001 (2009).

[80] B. Toshmatov, C. Bambi, B. Ahmedov, Z. Stuchlík and J. Schee, “*Scalar perturbations of nonsingular nonrotating black holes in conformal gravity*”, *Phys. Rev. D* **96**, 064028 (2017).

[81] B. Toshmatov, A. Abdujabbarov, Z. Stuchlík, and B. Ahmedov, “*Quasinormal modes of test fields around regular black holes*”, *Phys. Rev. D* **91**, 083008 (2015).

[82] M. Momennia and S. H. Hendi, “*Quasinormal modes of black holes in Weyl gravity: electromagnetic and gravitational perturbations*”, *Eur. Phys. J. C* **80**, 505 (2020).

[83] C. Ding, “*Gravitational quasinormal modes of black holes in Einstein-aether theory*”, *Nucl. Phys. B* **938**, 736 (2019).

[84] M. S. Churilova and Z. Stuchlik, “*Ringing of the regular black-hole/wormhole transition*”, *Class. Quantum Grav.* **37**, 075014 (2020).

[85] M. S. Churilova, R. A. Konoplya, and A. Zhidenko, “*Arbitrarily long-lived quasinormal modes in a wormhole background*”, *Phys. Lett. B* **802**, 135207 (2020).

[86] J. L. Blzquez-Salcedo, S. Kahlen, and J. Kunz, “*Quasinormal modes of dilatonic Reissner-Nordström black holes*”, *Eur. Phys. J. C* **79**, 1021 (2019).

[87] K. A. Bronnikov and R. A. Konoplya, “*Echoes in brane worlds: Ringing at a black hole-wormhole transition*”, *Phys. Rev. D* **101**, 064004 (2020).

[88] D. S. Eniceicu and M. Reece, “*Quasinormal modes of charged fields in Reissner-Nordström backgrounds by Borel-Padé summation of Bender-Wu series*”, *Phys. Rev. D* **102**, 044015 (2020).

[89] X. C. Cai and Y. G. Miao, “*Quasinormal modes and spectroscopy of a Schwarzschild black hole surrounded by a cloud of strings in Rastall gravity*”, *Phys. Rev. D* **101**, 104023 (2020).

[90] G. Panotopoulos and Á. Rincón, “*Quasinormal modes of five-dimensional black holes in non-commutative geometry*”, *Eur. Phys. J. Plus* **135**, 33 (2020).

[91] B. Turimov, B. Toshmatov, B. Ahmedov, and Z. Stuchlík, “*Quasinormal modes of magnetized black hole*”, *Phys. Rev. D* **100**, 084038 (2019).

[92] B. Carter, “*Global Structure of the Kerr Family of Gravitational Fields*”, *Phys. Rev.* **174**, 1559 (1968).

[93] S. E. Vázquez and E. P. Esteban, “*Strong-field gravitational lensing by a Kerr black hole*”, *Nuovo Cimento Soc. Ital. Fis. 119B*, 489 (2004).

[94] A. Das, A. Saha and S. Gangopadhyay, “*Study of circular geodesics and shadow of rotating charged black hole surrounded by perfect fluid dark matter immersed in plasma*”, *Class. Quantum Grav.* **39**, 075005 (2022).

[95] V. Cardoso, et. al., “*Geodesic stability, Lyapunov exponents, and quasinormal modes*”, *Phys. Rev. D* **79**, 064016 (2009).

[96] N. J. Cornish and J. Levin, “*Lyapunov timescales and black hole binaries*”, *Class. Quantum Grav.* **20** 1649 (2003).

[97] V. V. Kiselev, “*Quintessence and black holes*”, *Class. Quantum Grav.* **20** (6), 1187 (2003).

[98] V. V. Kiselev, “*Quintessential solution of dark matter rotation curves and its simulation by extra dimensions*”, *arXiv: 0303031 [gr-qc]*.

[99] Z. Xu, X. Hou and J. Wang, “*Kerr-anti-de Sitter/de Sitter black hole in perfect fluid dark matter background*”, *Class. Quantum Grav.* **35**, 115003 (2018).

[100] A. Das, A. Roy Chowdhury and S. Gangopadhyay, “*Stability, quasinormal modes in a charged black hole in perfect fluid dark matter*”, *Class. Quant. Grav.* **41** (1), 015018 (2024).

[101] M. H. Li and K. C. Yang, “*Galactic dark matter in the phantom field*”, *Phys. Rev. D* **86**, 123015 (2012).

[102] X. Hou, Z. Xu and J. Wang, “*Rotating black hole shadow in perfect fluid dark matter*”, *JCAP* **12**, 040 (2018).

[103] S. Deser and P. van Nieuwenhuizen, “*Nonrenormalizability of the Quantized Einstein-Maxwell System*”, *Phys. Rev. Lett.* **32**, 245 (1974).

[104] J. R. Klauder, “*On the meaning of a non-renormalizable theory of gravitation*”, *Gen. Relat. Gravit.* **6**, 13–19 (1975).

[105] M. Reuter, “*Nonperturbative evolution equation for quantum gravity*”, *Phys. Rev. D* **57**, 971 (1998).

[106] M. Reuter and F. Saueressig, “*Quantum Gravity and the Functional Renormalization Group*”, (Cambridge University Press, Cambridge, England, 2019).

[107] R. Percacci, “*An Introduction to Covariant Quantum Gravity and Asymptotic Safety*”, (World Scientific, Singapore, 2017).

[108] A. Bonanno and M. Reuter, “*Renormalization group improved black hole spacetimes*”, *Phys. Rev. D* **62**, 043008 (2000).

[109] J.M. Pawłowski and D. Stock, “*Quantum Improved Schwarzschild-(A)dS and Kerr-(A)dS Spacetimes*”, *Phys. Rev. D* **98**, 106008 (2018).

[110] A. Platania, “*From renormalization group flows to cosmology*”, *Front.in Phys.* **8**, 188 (2020).

[111] M. Reuter and H. Weyer, “*Running Newton constant, improved gravitational actions, and galaxy rotation curves*”, *Phys. Rev. D* **70**, 124028 (2004).

[112] U. Harst and M. Reuter, “*QED coupled to QEG*”, *J. High Energy Phys.* **05**, 119 (2011).

[113] A. Eichhorn and F. Versteegen, “*Upper bound on the Abelian gauge coupling from asymptotic safety*”, *J. High Energy Phys.* **01**, 030 (2018).

[114] A. Ishibashi, N. Ohta and D. Yamaguchi, “*Quantum improved charged black holes*”, *Phys. Rev. D* **104**, 066016 (2021).

[115] K. Jusufi, “*Quasinormal modes of black holes surrounded by dark matter and their connection with the shadow radius*”, *Phys. Rev. D* **101**, 084055 (2020).

[116] S. Fernando and J. Correa, “*Quasinormal modes of the Bardeen black hole: Scalar perturbations*”, *Phys. Rev. D* **86**, 064039 (2012).

[117] G. B. Arfken and H. J. weber, “*Mathematical Methods for Physicists*”.

- [118] N. Zettilli, “*Quantum Mechanics, 2ed: Concepts and Applications*”, John Willy and Sons Ltd., Chichester (2009).
- [119] D. J. Griffiths, “*Introduction to Quantum Mechanics. 2nd Edition*”, Benjamin Cummings (2004).
- [120] C. M. Bender and S. A. Orszag, “*Advanced Mathematical Methods for Scientists and Engineers I*”, Springer, United States of America (1999).
- [121] V. Cardoso and J. P. S. Lemos, “*Quasinormal modes of Schwarzschild-anti-de Sitter black holes: Electromagnetic and gravitational perturbations*”, *Phys. Rev. D* **64**, 084017 (2001).
- [122] C. Molina, A. B. Pavan, and T. E. Medina Torrejón, “*Electromagnetic perturbations in new brane world scenarios*”, *Phys. Rev. D* **93**, 124068 (2016).